Electronic Supplementary Material (ESI) for Energy & Environmental Science.

Supporting Information

Photosynthesis of Formate from CO_2 and Water at 1% Energy Efficiency via Copper Iron Oxide Catalysis

Unseock Kang,[1] Sung Kyu Choi,[2] Dong Jin Ham,[3] Sang Min Ji,[3] Wonyong Choi,[4] Dong Suk Han,[5] Ahmed Abdel-Wahab,[5] and Hyunwoong Park[1,*]

[1]School of Energy Engineering and [2]Department of Physics, Kyungpook National University, Daegu 702-701, Korea

[3]Energy Laboratory, Materials R&D Center, Samsung Advanced Institute of Technology, Samsung Electronics Co., LTD, Yongin 446-712, Korea

[4]School of Environmental Science and Engineering, POSTECH, Pohang, 790-784, Korea

[5]Chemical Engineering Program, Texas A&M University at Qatar, Education City, Doha, P.O. Box 23874, Qatar

Materials and Methods

Fabrication of electrodes

Pieces of fluorine-doped SnO_2 (F:SnO_2, FTO)-coated glass (Pilkington, ~50-nm-thick FTO layer, 1.5 cm × 3 cm) were cleaned ultrasonically in ethanol for 10 min, rinsed with distilled water and dried. For fabrication of $CuFeO_2$ and $CuFeO_2$/CuO electrodes, FTO substrates (active areas exposed to solution: 0.5 cm × 0.5 cm) were maintained at –0.36 V vs. SCE (saturated calomel electrode) for 2 h due to the highest efficiency in aqueous $KClO_4$ (50 mM, Aldrich) solution with $Cu(NO_3)_2 \cdot 3H_2O$ (4 mM, Aldrich) and $Fe(ClO_4)_3 \cdot H_2O$ (12 mM, Aldrich) using a potentiostat/galvanostat (Ivium). Platinum gauze was used as a counter electrode. After drying in air, as-deposited samples were annealed at 650°C for 3 h in Ar and air, resulting in formation of $CuFeO_2$ and $CuFeO_2$/CuO, respectively. Copper oxides (Cu_2O and CuO) were also fabricated using the same electrodeposition procedure in aqueous $KClO_4$ (50 mM, Aldrich) solution with $Cu(NO_3)_2 \cdot 3H_2O$ (4 mM, Aldrich). These samples were annealed at 650°C for 3 h in Ar and air, creating pure Cu_2O and CuO, respectively.

Photoelectrochemical test and product analysis

The photoelectrochemical (PEC) property of as-fabricated electrodes was examined in a three-electrode system with SCE and Pt gauze (or foil) as the reference and counter electrodes, respectively, using a potentiostat/galvanostat (Ivium) in aqueous potassium bicarbonate ($KHCO_3$, 0.1 M, Aldrich). If necessary, a high purity (> 99.99%) gas (O_2, N_2, Ar, or CO_2) was purged through the electrolyte for an hour prior to or continuously during the PEC test. A simulated solar light (AM 1.5G; 100 $mW \cdot cm^{-2}$) generated from a 150-W xenon arc lamp (ABET

technology) was irradiated to the backside of the electrodes (side not facing the electrolyte). During irradiation (continuous or chopped lights), potentials were swept from +0.4 to –0.5 V vs. SCE at a scan rate of 50 mV·sec^{-1}. For electrochemical characterization of the materials and bulk electrolysis, constant potentials (PEC-1) or constant currents were applied to the working electrodes. Faradaic efficiencies for formate production under constant currents (–0.2, –0.3, and –0.5 mA) were estimated using the following equation:

$$Faradaic\ efficiency\ (\%) = \frac{Formate\ (mol) \times (6.02 \times 10^{23})}{I\ (A) \times 1/96{,}485\ C^{-1} \cdot mol \times Time\ (s)} \times 2 \times\ 100\%.$$

If necessary, open-circuit potential (E_{OCP}) was recorded with time while neither potential nor current were applied (PEC-2). In the use of the potentiostat/galvanostat analytical instrument, the potentials with respect to SCE (V_{SCE}) were converted to those with respect to reversible hydrogen electrode (V_{RHE}) using the following relationship (*1*):

$$V_{RHE} = V_{SCE} + 0.241 + 0.059 \times pH.$$

Notably, the pH of air-equilibrated bicarbonate (0.1 M) solution is ~8.2, whereas CO_2-purging decreases the pH of bicarbonate to ~6.5. These pH changes were reflected when converting V_{SCE} to V_{RHE}.

The PEC performance of sample electrodes was further evaluated with a two-electrode configuration. The sample electrodes were directly wired to Pt foil at a distance of ~3 mm in a single (non-divided) air-tight glass reactor containing aqueous bicarbonate solution (0.1 M) with CO_2 purging for 1 h prior to or continuously during irradiation. No external bias was applied to the couples. While the cell voltages (E_{cell}) were recorded with a potentiostat/galvanostat (PEC-3) or digital multi-meter (Agilent 34401A) (PEC-4), solution and headspace gases were intermittently sampled and analyzed. In PEC-3, the working electrode terminal was connected to

sample electrodes, while the reference and the counter electrode terminals were connected to Pt foil. With this two-electrode system (PEC-3 and 4), solar-to-formate (STF) energy conversion efficiency was estimated using the following equation:

$$STF\ efficiency\ (\%) = \frac{Formate\ (mol) \times\ \Delta G^{\circ}\left(kJ \cdot mol^{-1}\right)}{P_{total}\left(mW \cdot cm^{-2}\right) \times Electrode\ area\ \left(cm^{2}\right)}$$

where ΔG° is the Gibbs free energy for conversion of gaseous CO_2 to liquid formate (270.14 $kJ{\cdot}mol^{-1}$) and P_{total} is the power of incident light (100 $mW{\cdot}cm^{-2}$). ΔG° was estimated based on the following chemical reaction: $CO_2(g) + H_2O(l) \rightarrow HCOOH(l) + 0.5O_2(g)$.

The headspace gases and solutions were analyzed intermittently during PEC tests. Initially, we examined the solution samples using gas chromatography mass spectroscopy (GC-MS, Agilent 7890 and MSD-5975C) and did not observe methanol and formaldehyde. The headspace gases were analyzed with GC-TCD (Agilent 7820) and GC-FID (Young Lin ACME 6100 and Agilent 7820); however, H_2, CO, and CH_4 were not observed (or below the detection limit if produced). Molecular oxygen (O_2) was found to be the measurable sole product in the headspace and was quantified using GC-TCD (Agilent 7820). In the solution phase, formate was identified and quantified using both high-performance liquid chromatography (HPLC, Young Lin 9100) and liquid chromatography (IC, Dionex ICS-1100). In HPLC analysis, a mixed eluent of distilled water and phosphoric acid (0.1 vol. %) flowed through a C18-inverse column (4.6 mm × 150 mm, Thermo) at 1 $mL{\cdot}min^{-1}$. In IC analysis, a mixed eluent of Na_2CO_3 (3.5 mM) and $NaHCO_3$ (1 mM) flowed through a Dionex IonPac AS 14 (4 mm × 250 mm) column.

Conversion of CO_2 gas to formate was confirmed using isotope tests using a nuclear magnetic resonance (NMR) spectrometer (Avance III 500 MHz, Bruker). Two separate PEC

experiments (PEC-4) were carried out in $^{13}CO_2$-purged bicarbonate (0.1 M) solution and CO_2-purged ^{13}C-labelled bicarbonate ($HO^{13}COO^-$, 0.1 M) solution for ^{13}C-NMR and H-NMR analyses. During PEC tests, a fraction of the solution (0.4 mL) was sampled intermittently and mixed with deuterium oxide (D_2O, 99.9%, Sigma) solution (1 mL) in NMR tubes (Norell, 5 mm-ultra precision). In addition, oxygen evolution from water was examined with the same PEC setup using ^{18}O-labelled water ($H_2{}^{18}O$, 20 vol. % in H_2O) as a solvent in which bicarbonate salt was dissolved (0.1 M) and CO_2 gas was purged. Selective ion-monitoring (SIM) GC-MS (Agilent 7890 and MSD-5975C) was used to analyze O_2 and ^{18}O-labelled O_2 ($^{32}O_2$, $^{34}O_2$, and $^{36}O_2$).

Electrochemical and optical characterization

The incident photon-to-current efficiencies (IPCE) were estimated in aqueous bicarbonate (0.1 M) solution (purged with CO_2 for 1 h) using a typical three-electrode configuration. Monochromatic light was produced from a 300-W xenon lamp (Newport Oriel) by a CS 130 monochromator with a 10-nm band pass, and the output power was measured with a silicon photodiode detector (Newport) (*1*). The IPCE was then calculated from $(1240 \times I_{ph}) \times 100 / (P_{light} \times \lambda)$, where I_{ph} ($mA \cdot cm^{-2}$), P_{light} ($mW \cdot cm^{-2}$), and λ (nm) refer to the photocurrent density at –0.5 V vs. SCE (+0.15 V vs. RHE), photon flux, and wavelength, respectively. For determination of flat band potential (E_{fb}), Mott-Schottky measurements were carried out through application of various potentials of –0.6 to +1.4 V vs. SCE (0 to +2 V vs. RHE) in bicarbonate solution (0.1 M) (purged with CO_2 for 1 h) at a frequency range of 0.1 kHz to 1 kHz (Gamry Instrument).

Sample electrodes were analyzed with X-ray diffraction (XRD, Rigaku D/Max-2500) and X-ray photoelectron spectroscopy (XPS, VG scientific, ESCA LAB 220i XL) using Mg Kα

lines (1253.6 eV) to examine the crystalline patterns of samples and the binding states of sample elements, respectively. A field emission scanning electron microscope (FE-SEM, Hitachi S-4800) equipped with an energy-dispersive X-ray (EDX) spectrometer was also employed to analyze the morphologies of samples and elemental mapping. The cross-section morphology and composition of $CuFeO_2$/CuO were analyzed with a focused ion beam (FIB, Hitachi, NB-5000) and high-resolution transmission electron microscope (HR-TEM, Hitachi, HF-3300) equipped with an EDX spectrometer. Nickel grid (Ted Pella, Inc., Pelco 200 mesh, 3.0 mm O.D.) was used for the TEM analysis. The optical absorption spectra of sample powders (collected from FTO) were recorded with a UV-Vis spectrophotometer equipped with a diffuse reflectance attachment (Shimadzu). All sample powders were mixed with $BaSO_4$ (sample: $BaSO_4$ = 1 : 9 by weight) and referenced to $BaSO_4$ (Sigma, > 99%).

Reference

1. S. K. Choi, W. Choi, H. Park, *Phys. Chem. Chem. Phys.* **15**, 6499 (2013).

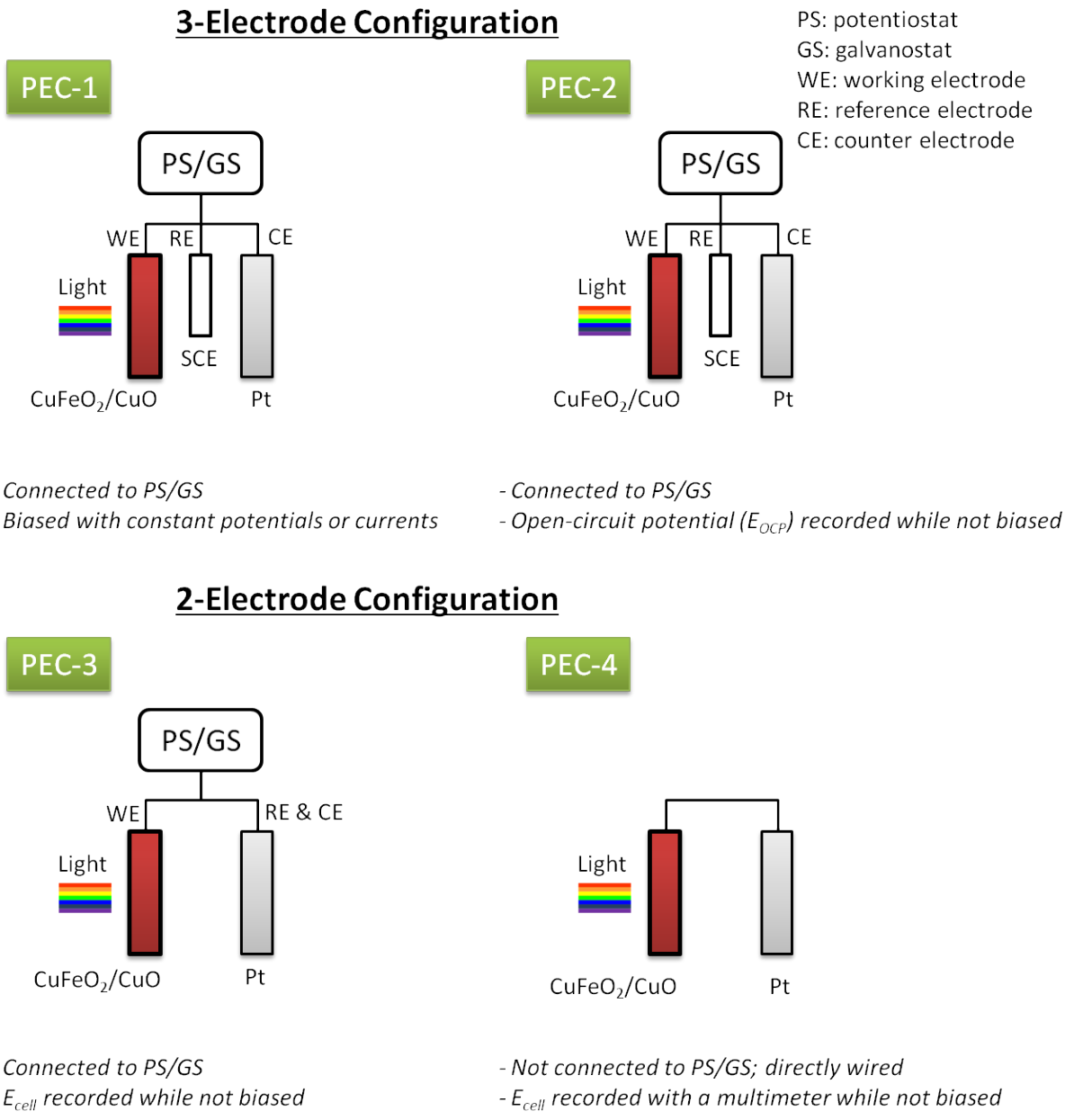

Scheme S1. Illustration for photoelectrochemical setups (PEC-1, 2, 3, and 4).

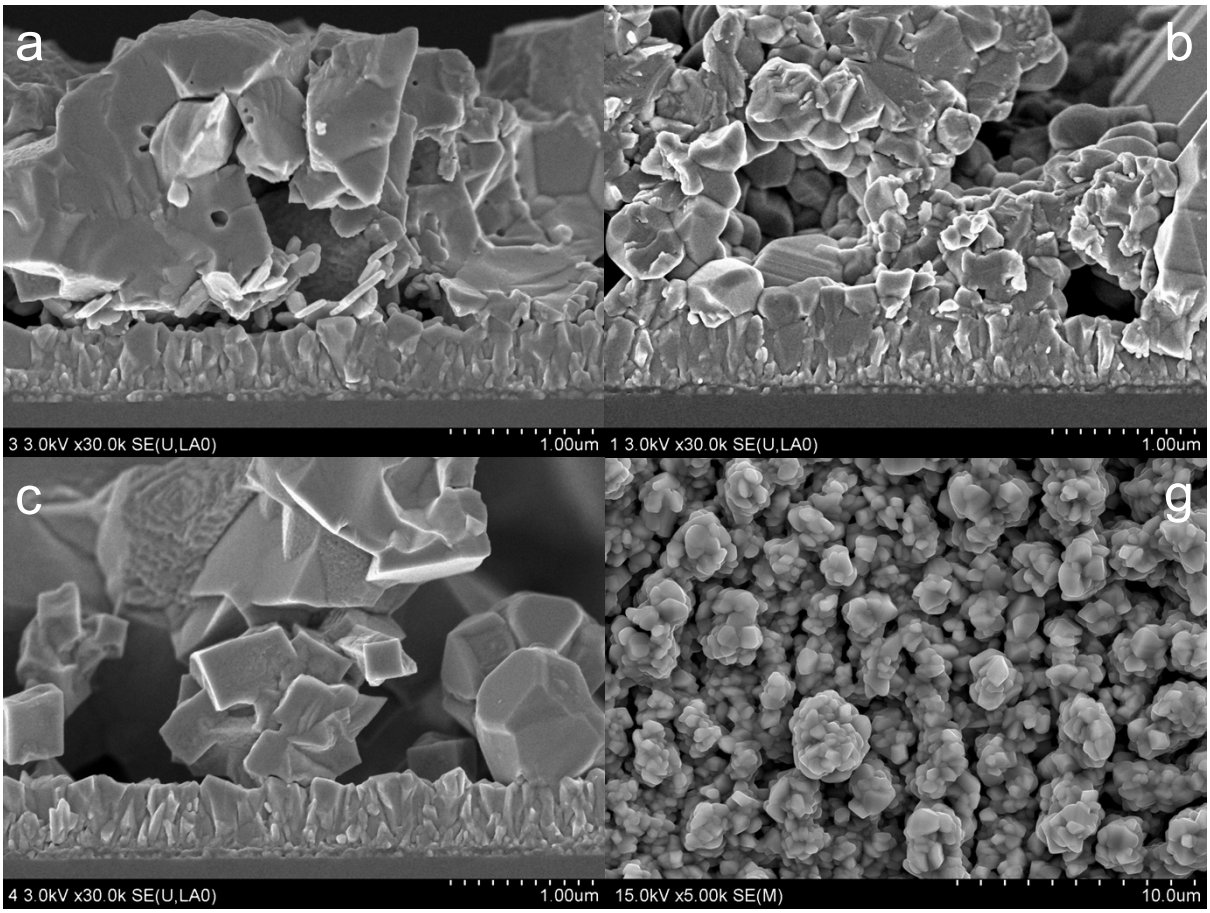

Figure S1. (a – c) Cross-sectional and (d) top views of SEM surface analyses for (a) CuO, (b) $CuFeO_2$, (c) Cu_2O, and (d) $CuFeO_2$/CuO electrodes electrodeposited on FTO at –0.36 V_{SCE} for 2 hours and annealed under air or Ar atmospheres at 650 °C for 3 hours.

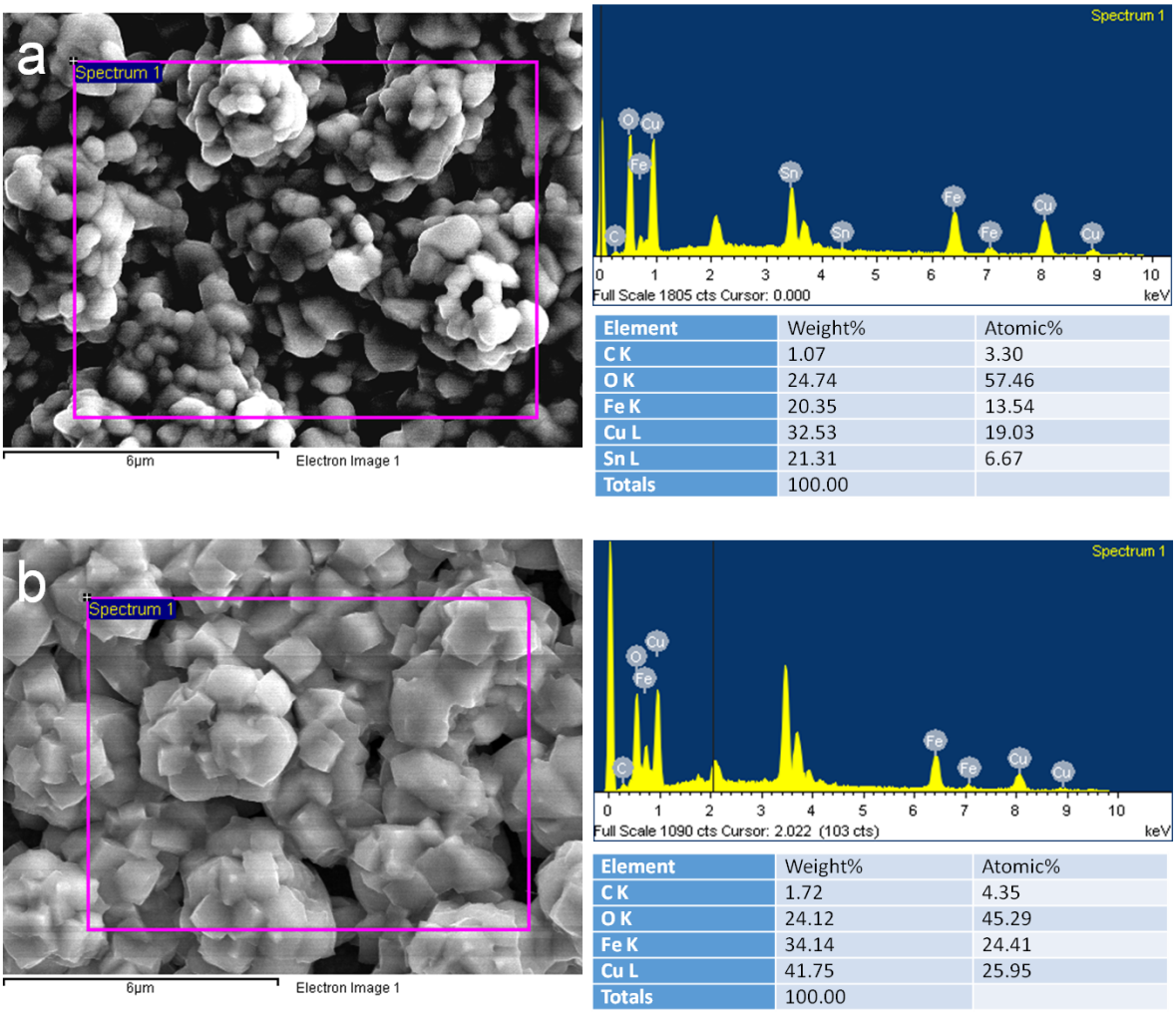

Element	Weight%	Atomic%
C K	1.07	3.30
O K	24.74	57.46
Fe K	20.35	13.54
Cu L	32.53	19.03
Sn L	21.31	6.67
Totals	100.00	

Element	Weight%	Atomic%
C K	1.72	4.35
O K	24.12	45.29
Fe K	34.14	24.41
Cu L	41.75	25.95
Totals	100.00	

Figure S2. SEM and EDX elemental analyses of (a) $CuFeO_2$/CuO and (b) $CuFeO_2$. They were grown on FTO via an electrodeposition for 2 hours and annealed at 650 °C for 3 hours under air and Ar atmospheres, respectively.

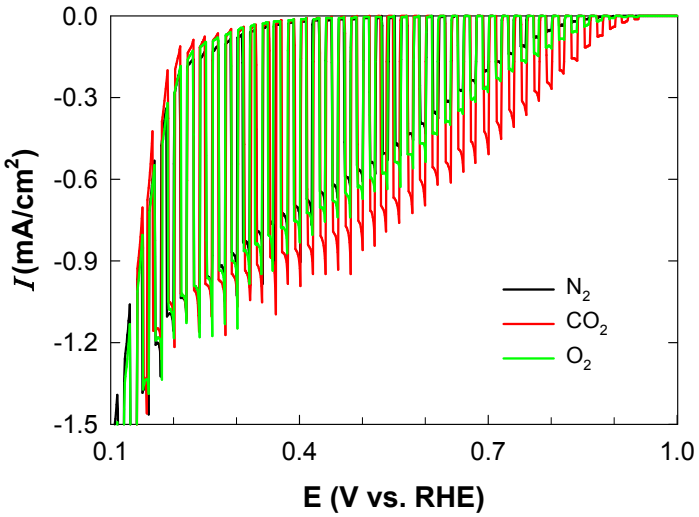

Figure S3. Light-chopped linear sweep voltammograms of $CuFeO_2$/CuO electrodes in 0.1 M bicarbonate solutions purged with different gases. Nitrogen and oxygen purging insignificantly changed the solution pH of ~8.2, whereas CO_2 purging decreased the pH to ~6.5. This pH effect was reflected in converting SCE to RHE.

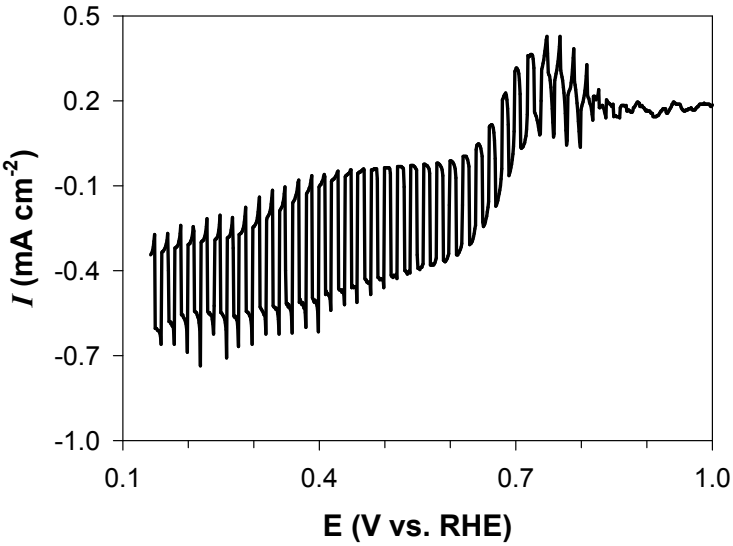

Figure S4. Light-chopped linear sweep voltammogram of Cu_2O electrode in 0.1 M bicarbonate solution purged with CO_2.

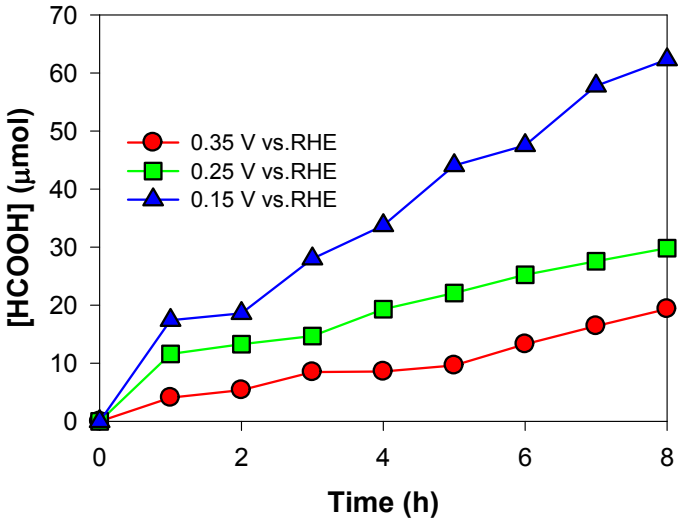

Figure S5. Time-profiled formate generations with $CuFeO_2$/CuO electrodes at varying E_{bias}s in CO_2-purged bicarbonate (0.1 M) solution.

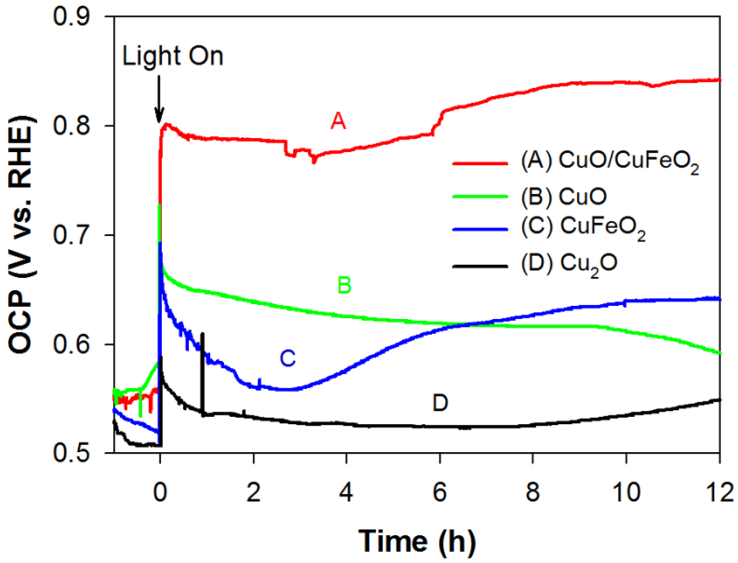

Figure S6. Time-profiled changes in open circuit potentials (E_{ocp}) of sample electrodes in CO_2-purged bicarbonate (0.1 M) solution under irradiation (PEC-2).

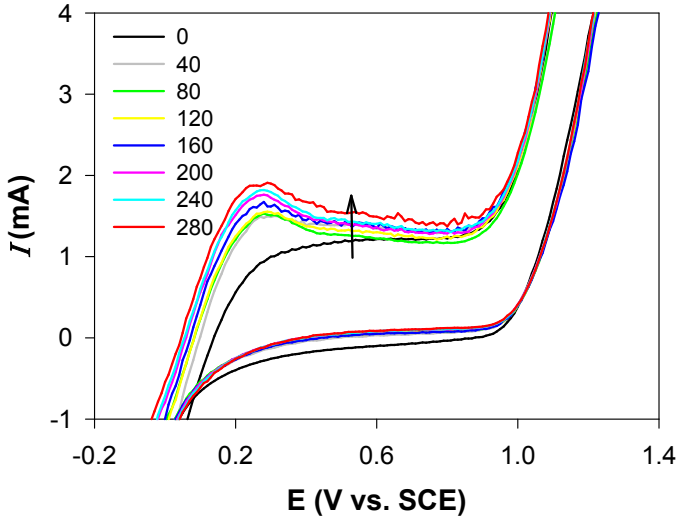

Figure S7. Cyclic voltammograms of Pt foil in 0.1 M bicarbonate solution including varying amounts of formate (μmol). Note that the first anodic bands at ~0.27 V_{SCE} were intensified with increasing the amount of formate, whereas the second ones beginning at ~0.9 V_{SCE} were less influenced. They are attributed to the oxidations of formate and water, respectively.

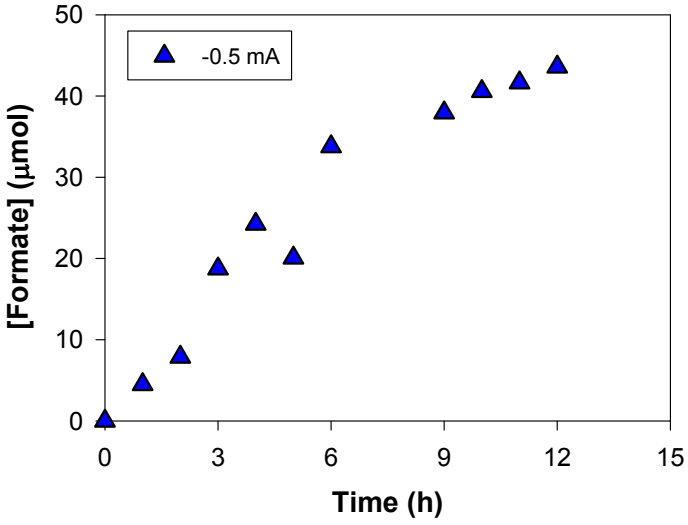

Figure S8. Galvanostatic generation of formate with irradiated $CuFeO_2$/CuO at I = –0.5 mA in CO_2-purged bicarbonate solution.

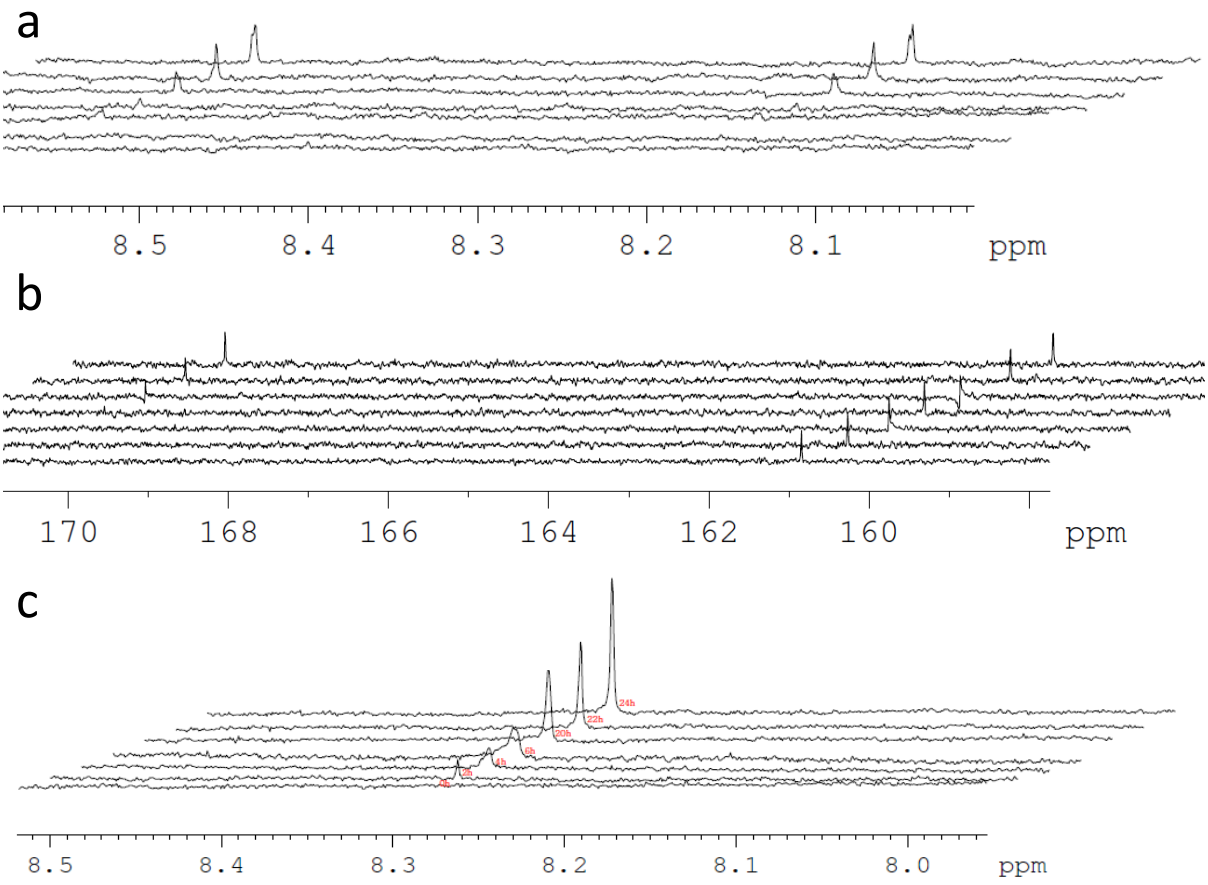

Figure S9. (a) ^{1}H-NMR and (b) ^{13}C-NMR observations of $H^{13}COO^{-}$ produced from $^{13}CO_2$ purged in $H^{12}CO_3^{-}$, and (c) ^{1}H-NMR observations of $H^{12}COO^{-}$ produced from CO_2 purged in $H^{13}CO_3^{-}$ with irradiated $CuFeO_2$/CuO and Pt couple (two-electrode system). Irradiation times: 0, 2, 4, 6, 20, 22, and 24 hours from the bottom

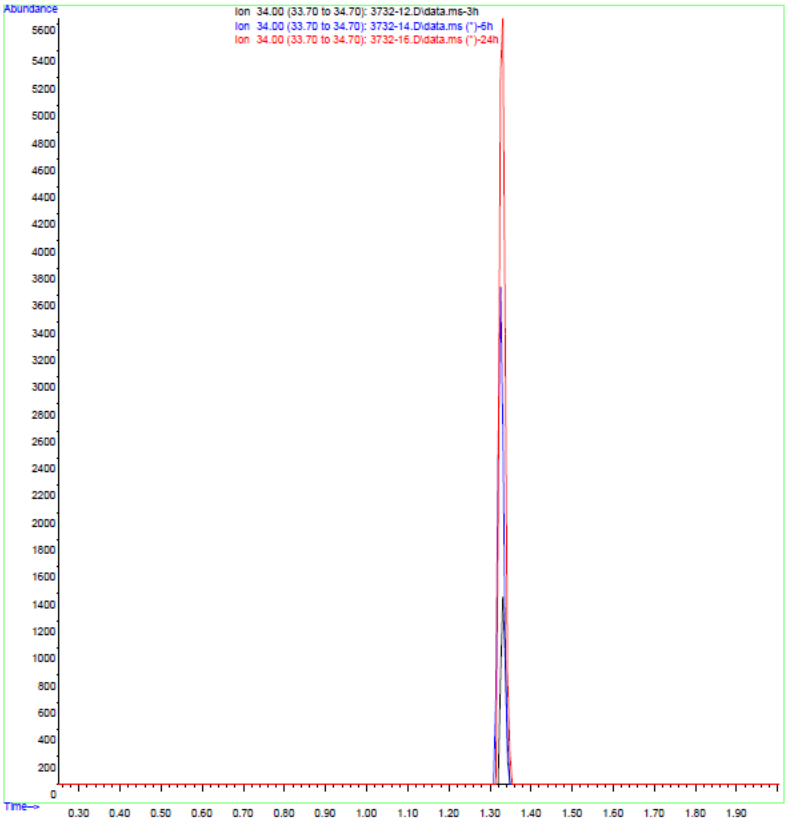

Figure S10. GC-MS spectra for $^{34}O_2$ produced from $^{18}O_2$-labelled water (H_2O^{36}/H_2O^{32} = 1/4 v/v; 0.1 M bicarbonate) with irradiated $CuFeO_2$/CuO and Pt couple (PEC-4).

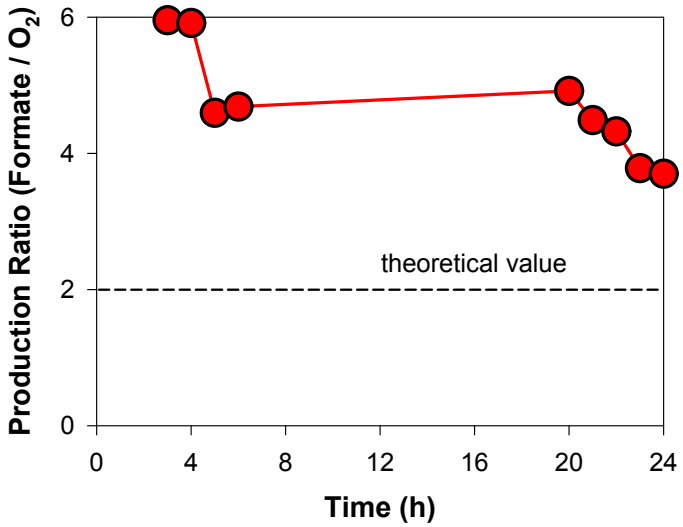

Figure S11. Production ratios of formate and O_2 with irradiated $CuFeO_2$/CuO and Pt couple (PEC-4).

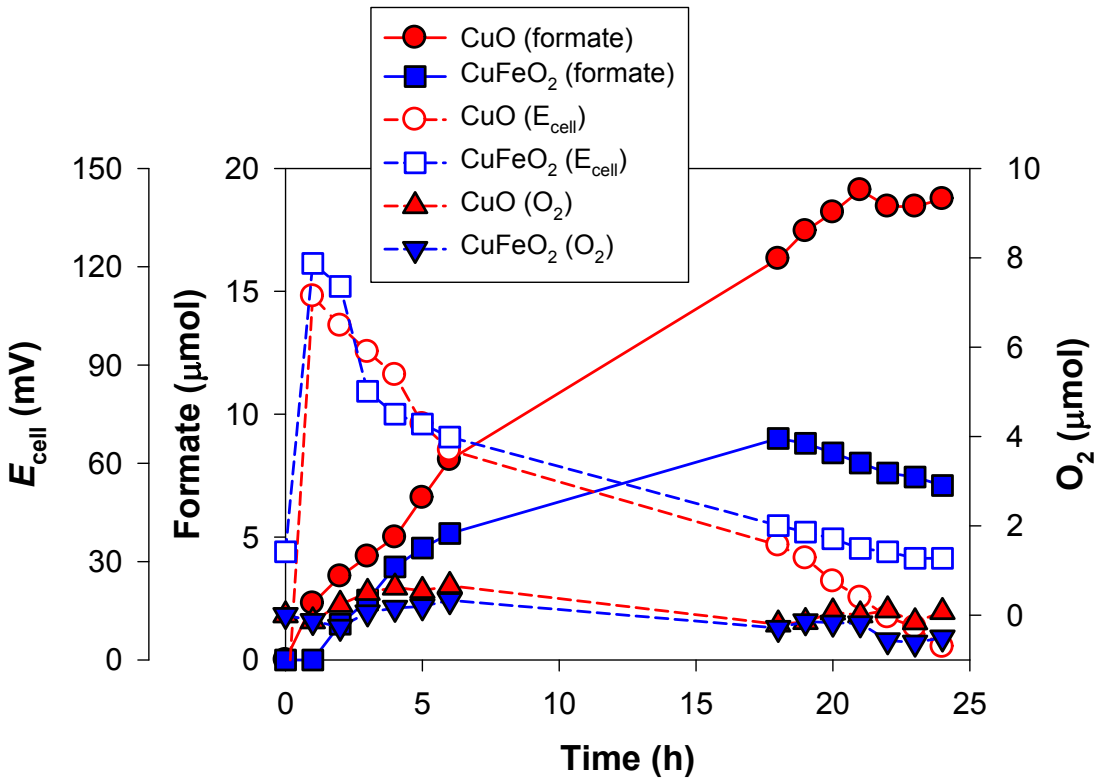

Figure S12. Time profiled changes in E_{cell}, formate production, and oxygen production in CO_2-purged bicarbonate (0.1 M) solution with irradiated CuO-Pt or $CuFeO_2$-Pt couples (PEC-4).

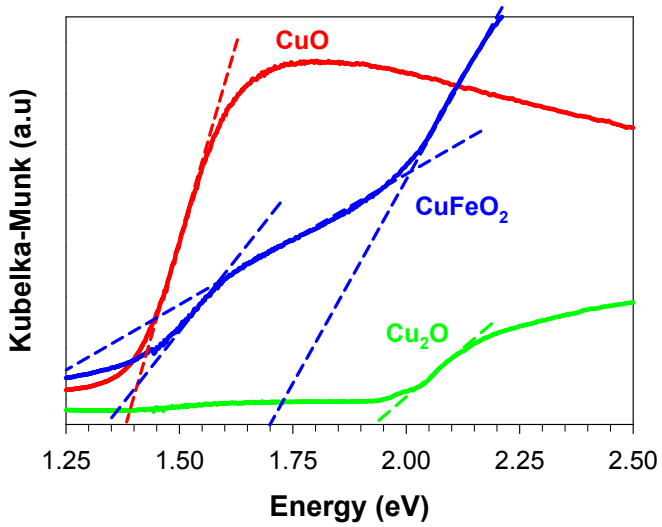

Figure S13. Diffuse reflectance UV-Vis absorption spectra of sample particles. The electrodeposited particles were collected as powders.

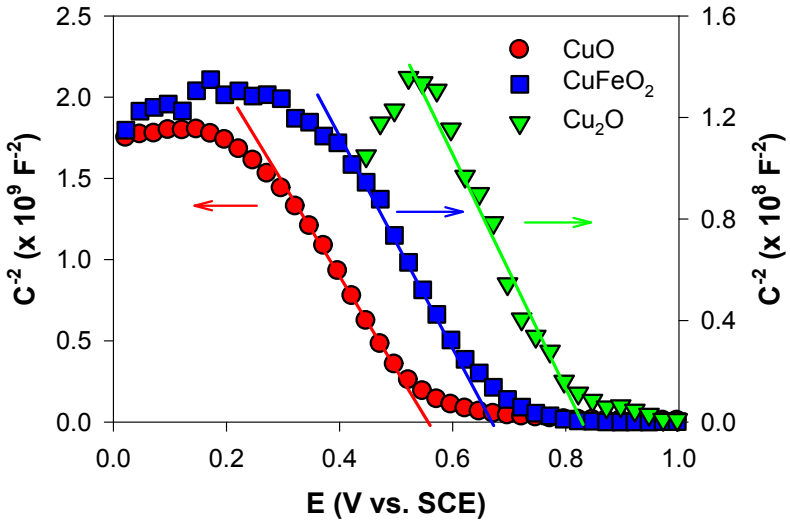

Figure S14. Mott-Schottky plots of CuO, $CuFeO_2$, and Cu_2O electrodes in CO_2-purged bicarbonate (0.1 M) solution.

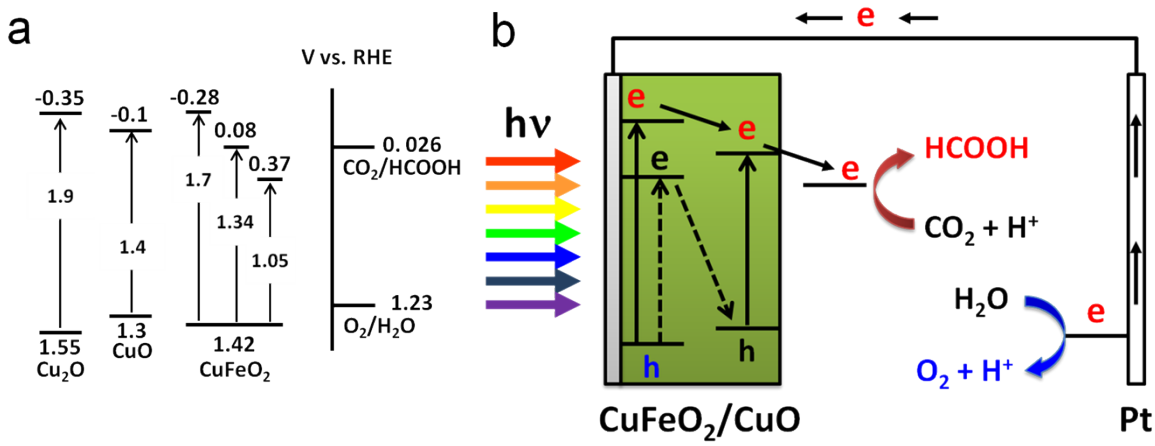

Figure S15. (a) Estimated diagram of the energetics of p-type semiconductor samples and the reduction potentials of CO_2 and O_2. Bandgap energies (eV, numbers on arrows) and flatband potentials were determined in Fig. S13 and S14, respectively, while the latter values were considered to be located approximately 100 mV above the potential of the valence band edge. Upper and lower bars refer to conduction and valence band edges, respectively, while the numbers above and below bars indicate energy levels (V vs. RHE). (b) Charge transfers occurring at $CuFeO_2$/CuO electrodes and overall chemical reactions. The 1.05 eV-band transition of $CuFeO_2$ was omitted for simplicity. Note that the work function (W_f) of Pt is 5.5 – 6 eV depending on the surface orientation and state (*CRC Handbook of Chemistry and Physics*, 90th ed., Florida, 2009). The conversion of electron volt (eV) to an electrochemical potential versus normal hydrogen electrode (V vs. NHE) is a challenge as well, because the conversion factor (χ) varies between –4.2 and –4.5 eV (i.e., V vs. NHE = $\chi - (-W_f/e)$; reflecting the spread in values of hydration enthalphies; see *Nature* 423 (2003) 626). With this limit, the electrochemical potential of Pt can be estimated to 1 V (lower limit) to 1.8 V (upper limit). The conduction band edge of CuO was determined to be –0.1 V, leading to the potential difference of 1.1 to 1.9 V.

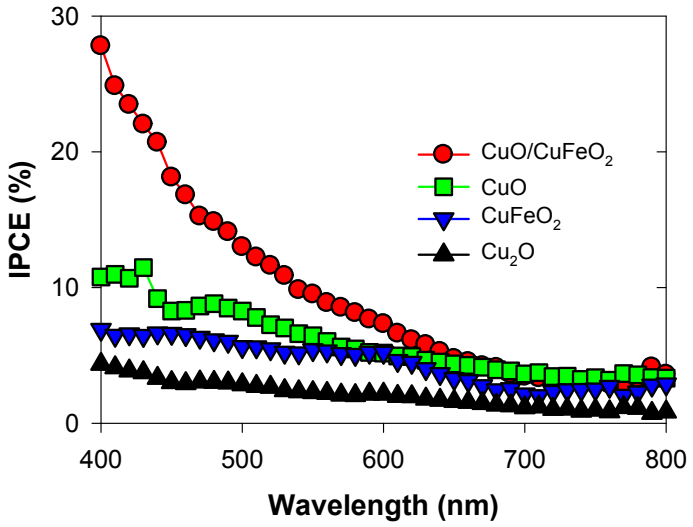

Figure S16. Incident photon-to-current efficiencies (IPCEs) of sample electrodes at +0.15 V_{RHE} in CO_2-purged bicarbonate (0.1 M) solution. IPCE values at $\lambda > 800$ nm were less reliable and omitted.

IPCE measurements were completed at constant potential bias of +0.15 V_{RHE} using the following equation.

$$IPCE\ (\%) = \frac{1240 \times J_{ph}\left(mA\ cm^{-2}\right)}{P_{light}\left(mW\ cm^{-2}\right) \times \lambda\ (nm)} \times 100\%$$

where, J_{ph}, P_{light}, and λ refer to the photocurrent density, photon flux, and wavelength, respectively.